THE ASTROPHYSICAL JOURNAL, 405:179–185, 1993 March 1

SOFT VARIABILITY AND REFLECTION FEATURES IN THE X-RAY SPECTRUM OF THE SEYFERT GALAXY NGC 5506

I. A. BOND, M. MATSUOKA, AND M. YAMAUCHI
Institute of Physical and Chemical Research (RIKEN), Wako, Saitama, 351-01, Japan
Received 1992 March 31; accepted 1992 September 8

ABSTRACT

Observations of the Seyfert 2 galaxy NGC 5506 obtained by *Ginga* in 1991 July 6–10, are presented. In addition to an iron emission line around 6.4 keV, soft excess emission below 3 keV and a hard tail-like feature are detected. On one episode on July 9, the spectrum softened, over a 5 hr time scale, to a maximum level after which it returned to the level seen on the other observation days. The softness variability may be described in terms of the partial covering model, while the high-energy feature is best described by a feature representing reflection by cold, dense matter. On July 6 and 10, the covering fraction was ~80%, but on July 9 this value declined to a minimum value of ~60%. While we do not rule out the presence of ionized matter, the lack of correlation of the spectral softness with the continuum flux rules out models based on photoionization as the softness variability mechanism. It is suggested that this mechanism resides in the inner accretion disk where the dip in the apparent covering fraction is due to instabilities in the accretion flow.

Subject headings: accretion, accretion disks — galaxies: individual (NGC 5506) — galaxies: Seyfert — X-rays: galaxies

1. INTRODUCTION

It is well known that the spectra of Seyfert galaxies in the 1–30 keV range generally have a complex structure and cannot be described by a simple canonical power law with uniform absorption. In addition to the iron K emission line around 6.4 keV, detected in virtually all Seyfert spectra, there are several other features which complicate the simple model.

Observations by the *Einstein*, *EXOSAT*, and *Ginga* satellites had shown that a large fraction of Seyfert spectra exhibit a "soft excess" emission, at ~2 keV, above that predicted by the simple model (e.g., Urry et al. 1989; Turner & Pounds 1989). These observations show that the form of the soft excess is different from object to object and is suggestive of a variety of physical origins. Models which had been successfully applied include partial covering where the soft excess arises from leakage of the power-law source through a spatially nonuniform absorption screen (e.g., NGC 4151; Holt et al. 1980; Perola et al. 1986; Yaqoob & Warwick 1991; NGC 6814; Yamauchi et al. 1992) and blackbody emission or thermal bremsstrahlung associated with the inner regions of an accretion disk (e.g., MCG −6-30-15; Turner et al. 1991). In a recent reanalysis of the X-ray spectra of 25 Seyfert spectra obtained by *Einstein*, Turner et al. (1991) consider a blend of iron L, oxygen K, and neon K shell emission lines as a possible explanation of soft excess emission.

The Large Area Counter on board *Ginga* revealed the presence of a hard tail above 10 keV in several Seyfert spectra. Previously, Guilbert & Rees (1988) and Lightman & White (1988) had shown that sufficiently dense, cold matter may coexist within the hard X-ray emitting region. The cold matter reprocesses the hard X-ray spectrum via fluorescence, Compton reflection, and photoabsorption producing an iron emission line at 6.4 keV and a hard tail. This so-called reflection model has been successfully applied to the individual X-ray spectra of NGC 7469 and IC 4329A (Piro, Yamauchi, & Matsuoka 1990) and NGC 4051 (Matsuoka et al. 1990). The reflection model has also been applied to a composite spectrum of 12 Seyfert galaxies by *Ginga* (Pounds et al. 1990) and has been used in models dealing with an AGN origin of the X-ray background (Morisawa et al. 1990; Fabian et al. 1990; Terasawa 1991).

NGC 5506 is bright Seyfert 2 galaxy at a cosmological redshift of 0.0061. On an analysis of data obtained previously by *Ginga* and *EXOSAT*, Pounds et al. (1989) showed that the spectrum may be fitted by a model comprising an absorbed power law, an iron fluorescence line at 6.4 keV, and an iron K-absorption edge at 8.3 keV. The last feature indicates ionized gas in the line of sight. These observations along with earlier observations by *Einstein* (Turner et al. 1991) showed little or no signs of a soft excess. Here we report recent *Ginga* observations of NGC 5506 and show a soft excess to be clearly present and clearly variable. We then consider various models in explaining the soft excess and its variability. We also find that the hard region of the spectrum is better described in terms of the reflection model rather than a K-edge feature.

2. OBSERVATIONS AND DATA REDUCTION

NGC 5506 was observed by *Ginga* as a "target of opportunity" on 1991 July 5–10. The observations were performed with the Large Area Counter (LAC) on board the satellite. This instrument comprises eight proportional counters with a total area of 4000 cm^2 and a FWHM energy resolution of 18% at 6 keV (Turner et al. 1989). Data acquisition was carried out in "MPC-1" mode which provides full spectral resolution in 48 channels over the 1.2–37 keV range.

On-source observations were carried out on July 6, 8, 9, and 10. The observations of July 8 were of low collimator efficiency (<60%) due to pointing problems of the satellite and are not included in the spectral analysis. Background observations were carried out on July 5 and 7 where the satellite was pointed at a "blank-sky" region. During these observations the Sun was behind the field of view of the LAC and contamination by solar X-rays is not expected to be a problem. Background subtraction was carried out on an orbit by orbit basis. For a given orbit corresponding to an on-source observation, the background is given by a blank sky observation taken at the

same position in the orbit. The energy calibration was checked using the 22.1 keV Kα fluorescence line produced by the silver coating.

For both source and background observations, data corresponding to low geomagnetic rigidities (< 10 GeV/c) and low Earth elevation angles (< 5°) were excluded from the analysis. Furthermore, the analysis is restricted to "remote" orbits where the satellite does not pass through the South Atlantic Anomaly. Each orbit corresponds to 20–30 minutes continuous observing. On each day, *Ginga* makes five or six remote orbits. The corresponding SUD (surplus over upper discriminator equals the count rate above 37 keV) count rates for these orbits did not exceed 5 counts s^{-1} throughout all source and background observations. This indicates a very low and stable particle-induced background throughout the observation period.

3. FEATURES OF THE SPECTRUM

The integrated X-ray spectrum obtained from the observations of July 6, 9, and 10 was tested against a simple model comprising a single power law with uniform absorption by a cold cosmic abundance gas (cross section given by Morrison & McGammon 1983). The model was fitted over the 1.2–28 keV range of the spectrum. The reduced χ^2 value was 16.6., and it is clear that the spectrum cannot be represented by this model. As can be seen in Figure 1, the distribution of residuals from this simple model is dominated by an iron line feature and a low-energy excess below 3 keV. Also apparent is a hard bump above 10 keV.

TABLE 1

INTENSITY MEASUREMENTS OF NGC 5506

DATE (1991)	INTENSITY (counts s^{-1}) Total (1.2–28 keV)	Soft (1.2–3 keV)	Intermediate (3–10 keV)	Hard (10–28 keV)
Jul 6	28.5 ± 0.2	3.74 ± 0.09	22.5 ± 0.2	2.33 ± 0.07
Jul 8	28.3 ± 0.2	3.46 ± 0.08	22.5 ± 0.2	2.32 ± 0.07
Jul 9	30.8 ± 0.2	4.65 ± 0.09	23.8 ± 0.2	2.35 ± 0.07
Jul 10	46.1 ± 0.3	6.12 ± 0.11	36.5 ± 0.3	3.47 ± 0.08

The day-by-day intensities within various energy bands are summarized in Table 1. While the observations of July 8 are not used in the spectral analysis, the intensities, corrected for collimator response, are included in Table 1. The total intensity of NGC 5506 remained at around 30 counts s^{-1} from July 6 to 9 and increased slightly to around 45 counts s^{-1} between July 9 and 10. The structure of the spectra obtained separately on each observation day may be compared in a model-independent way in Figure 2. This is done by means of pulse height ratio plots which compares the count rate on July 6 and

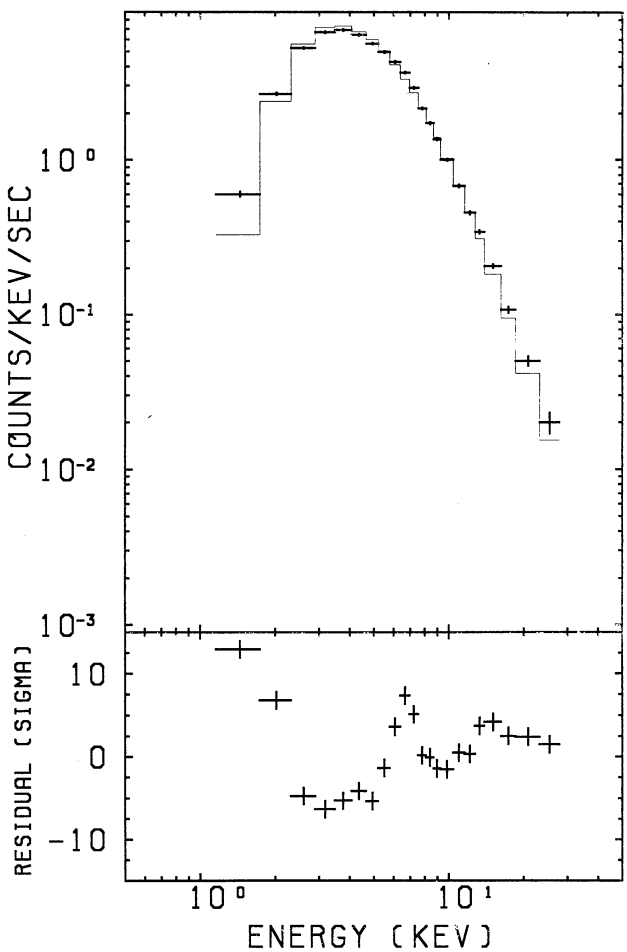

FIG. 1.—Spectral fitting to a simple power law with uniform absorption for the total spectrum obtained from the 1991 observations of NGC 5506.

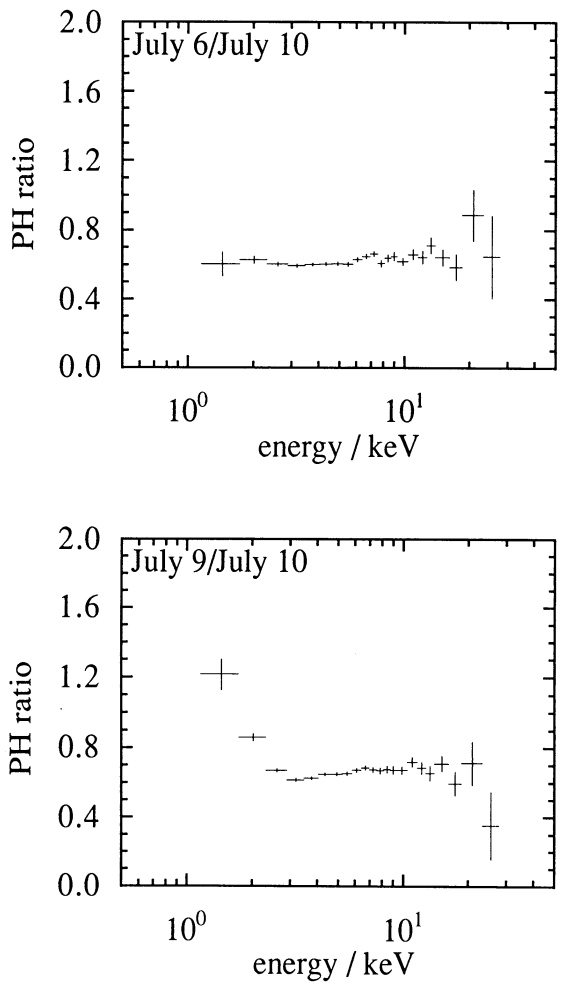

FIG. 2.—Ratio of count rate recorded by each energy channel on July 6 and 9 to the corresponding count rates recorded on July 10.

9 to that of July 10 on an energy channel by channel basis. Each spectrum is integrated over each orbit on the given observation day. The pulse height ratio plots clearly show a considerable softening of the spectrum on July 9, whereas the spectral structure on July 6 and 10 are similar.

We further examine for signs of spectral variability by dividing the spectrum into three energy bands: the soft band (1.2–3 keV), the intermediate band (3–10 keV), and the hard band (10–28 keV). The intermediate band may be used to represent the continuum emission (i.e., the absorbed power law). We then define the softness and hardness ratios as the intensities in the respective bands to that of the intermediate band. These quantities are calculated separately for each orbit. Spectral time variability is examined in Figure 3, where the soft, intermediate, and hard intensities are plotted along with the softness and hardness ratios. On July 9, a clear rise in the softness ratio followed by a drop can be seen.

The spectral variability seen on July 9 is examined in more detail in Figure 4. In Figure 4*b* the variation of the softness and hardness ratios with time are shown. The variability in the softness ratio can be seen to take place on a time scale of ~5 hr. The rise in the softness ratio also appears to be accompanied by a rise in the hardness ratio. However, the hardness ratio fluctuates on the other observation days on a scale similar to that seen on July 9. In Figure 4*a* the time variation of the soft, intermediate and hard fluxes are plotted. In can be seen that the increase in the softness and hardness ratios do arise from a differential increase in their respective fluxes rather than from a decrease in the intermediate flux. In Figure 5 the softness ratio versus the intermediate flux is plotted. This shows an important feature of the soft excess variability on July 9 in that the softness ratio does not follow variation in the continuum as represented by the intermediate flux.

False spectral variations may arise from a poor background subtraction. Here we assess the systematic errors that may be present due to a variable background. The blank field observations of July 5 yielded six remote orbits while those of July 7 yielded four remote orbits. The distribution over energy channels of rms values of the differences in count rates between adjacent orbits is shown in Figure 6. This shows the extent of the variability in the background on the time scale of the order of one orbit (~90 minutes). Figure 6 also indicates the maximum systematic errors that may be present in the back-

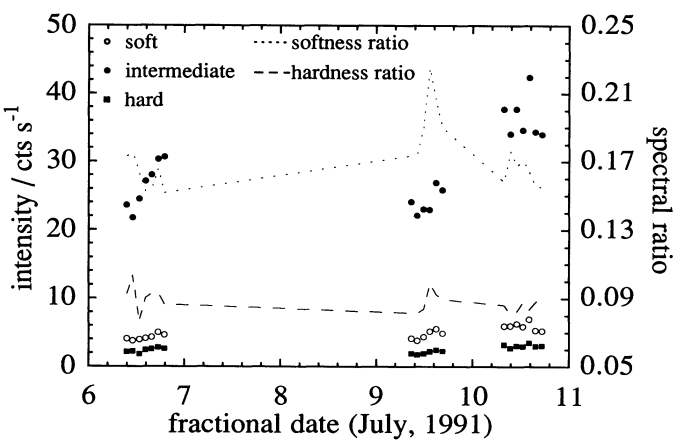

FIG. 3.—Spectral variability of NGC 5506 during 1991 July 6–10. The soft (1.2–3 keV), intermediate (3–10 keV), and hard (10–28 keV) X-ray intensities derived from each orbit are plotted along with the softness and hardness ratios.

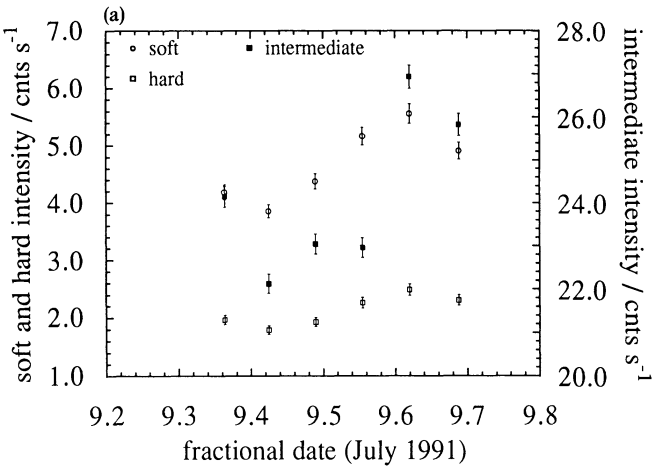

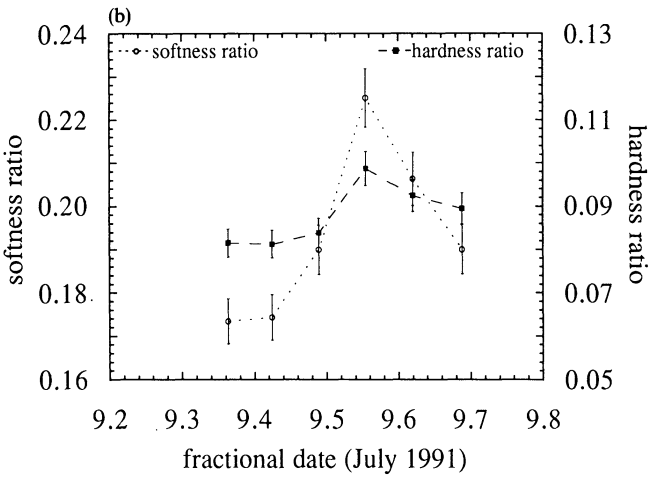

FIG. 4.—Spectral variability of NGC 5506 on 1991 July 9. (*a*) Soft (1.2–3 keV), intermediate (3–10 keV), and hard (10–28 keV) X-ray intensities and (*b*) softness and hardness ratios derived at each orbit plotted as a function of time.

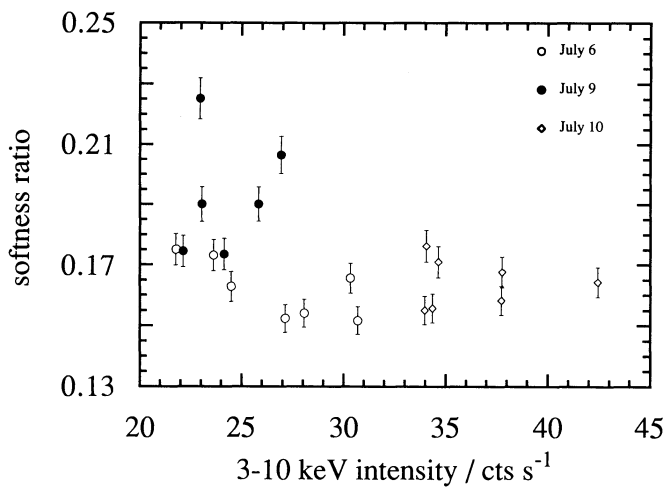

FIG. 5.—Soft color diagram based on intensity measurements obtained at each orbit corresponding to an on-source observation of NGC 5506. The measurements are grouped into observation day as follows: July 6 (*open circles*), July 9 (*filled circles*), and July 10 (*open diamonds*).

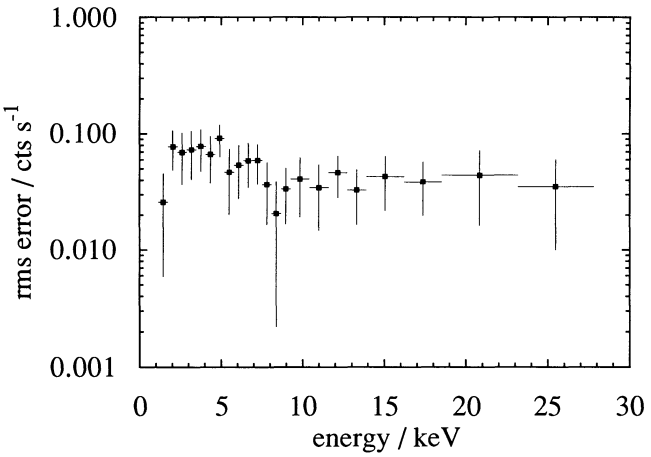

FIG. 6.—The distribution over energy channels of rms values of the differences in count rates between adjacent orbits of the blank field observations of 1991 July 5 and 7.

ground subtraction process. It can be seen that none of the rms values exceed 0.1 counts s^{-1} in any channel. By summing up these values over the respective energy bands in Figure 6, the rms values in the soft, intermediate, and hard bands are 0.17, 0.66, and 0.27 counts s^{-1}, respectively. These values represent the maximum systematic errors in the extreme case where the errors all have the same sign within their respective energy bands. If these errors were present then the softness and hardness ratios measured on July 9 would be affected by factors of 3.6% and 11%, respectively. It should be noted that these are worst case values and that systematic errors are considerably reduced by carrying out the background subtraction on an orbit by orbit basis. We thus consider it unlikely that the spectral variations seen here arise from a poor background subtraction.

4. MODEL FITTING

4.1. *Model Fitting above 3 keV*

First, we studied the features in the 3–28 keV range so as to avoid any complications introduced by the soft excess and its variability. For this purpose the total spectrum summed over the full observation period was used for greater statistics. The simple power law and absorption model fitted in this energy range gives an unacceptable reduced χ^2 value of 8.62 for 16 degrees of freedom (d.o.f.). An emission line, represented by a Gaussian profile, was then added to this model. The central energy and intensity were free parameters but the rms half-width was fixed at 0.1 keV. The residuals from this model are shown in Fig. 5*a*. A reduced χ^2 value of 2.13 was obtained with 14 d.o.f. This is a significant improvement at a confidence level greater than 99% as demonstrated by an *F*-test. The central energy was determined to be 6.33 ± 0.10 keV which becomes 6.37 ± 0.10 keV after correcting for the cosmological redshift of NGC 5506. This value is close to the 6.4 keV value characteristic of iron fluorescence within a cold gas. The equivalent width of the line was found to be 207 ± 34 eV.

While the fitting is considerably improved by the addition of an emission line, the resulting χ^2 is still not formally acceptable. Following Pounds et al. (1989) we investigated the presence of ionized matter. An iron *K*-edge feature was included in the above model with the edge energy fixed at the cold value of 7.1 keV. The line energy was fixed at the cold value determined above. The resulting reduced χ^2 value of 1.6 for 14 d.o.f. is only marginally acceptable. The edge energy was then allowed to be a free parameter. An acceptable fit was obtained with a reduced χ^2 value of 1.1 for 13 d.o.f. The residuals are shown in Figure 7*b*. The power-law index was determined to be 1.83 ± 0.04 and the hydrogen column density of the absorbing screen was found to be $(1.3 \pm 0.08) \times 10^{22}$ cm^{-2}. These values are in close agreement with those derived from the same model applied by Pounds et al. to the previous *Ginga* observation of NGC 5506. The best-fitted edge energy was 8.0 ± 0.4 keV, a little lower than the value of 8.3 keV obtained by Pounds et al. Our value for the edge energy along with its error imply an ionization level of iron from Fe XVIII to Fe XXI. Our results are consistent with that of Pounds et al. in that a similar level of ionization is implied. The iron overabundance factor derived from fitting the edge was 12 ± 7 relative to the cosmic value. Within error, this is in agreement with the value of 6 found by Pounds et al. The real overabundance would be less than this if, as implied by the warm edge energy, ionized matter is present. This is because of the reduced opacity at low energies which would result in the value of the hydrogen column (which

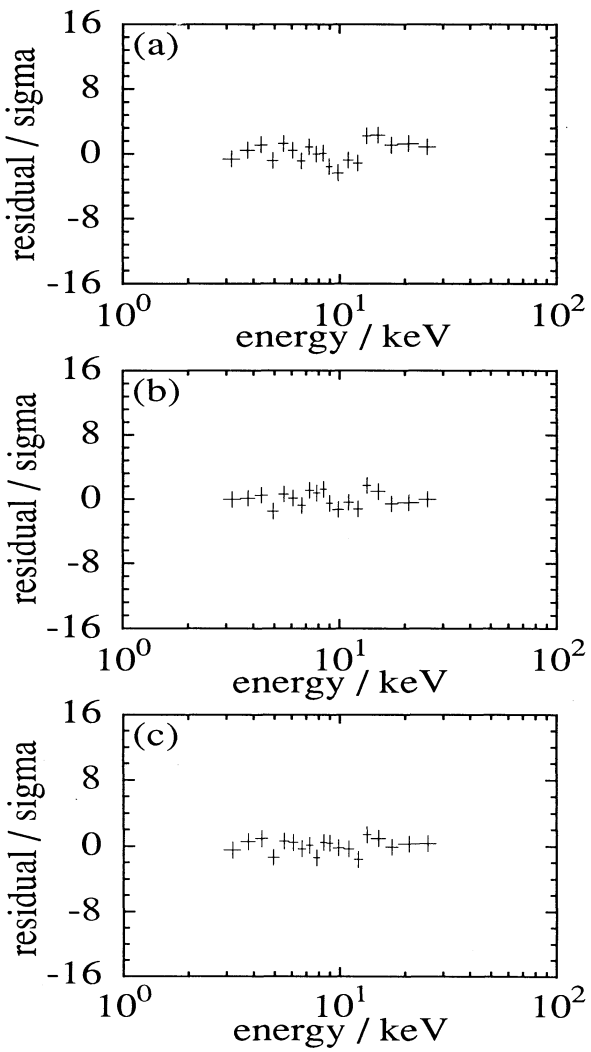

FIG. 7.—Residuals of the total spectrum from (*a*) uniformly absorbed power law plus emission line, (*b*) model (*a*) with a K-edge feature included, and (*c*) model (*a*) with a reflection feature included.

is derived on the assumption of a cold gas) being smaller than the real value.

Inspection of the residuals from the absorbed power law plus emission-line model in Figure 7*a* show a distinct hard tail. An alternative model was tried where, instead of a K-edge, a feature representing Compton reflection off cold, dense matter was included In this model, the power law is modified by the factor $1 + rA(E, \Gamma)$, where r is a normalization factor. The albedo, A, of the reflecting matter as a function of energy, E, and power-law index, Γ, was calculated after Lightman & White (1988). This model also results in an acceptable fit with a reduced χ^2 value of 0.9 for 14 d.o.f. The residuals are shown in Figure 7*c*. The inclusion of this reflection feature resulted in a steeper power-law index of 2.02 ± 0.09 as would be expected. Also a higher hydrogen column density of $(3.7 \pm 0.4) \times 10^{22}$ cm^{-2} was obtained. The normalization factor of the reflected component was 0.8 ± 0.4.

4.2. *Soft Excess–Partial Covering Models*

In the previous section, we established that the spectrum of NGC 5506 in the 3–28 keV range can well be fitted by two models which we shall refer to as the warm edge and reflection models, respectively. Here we extend the spectral fitting procedure to include the 1.2–28 keV range so as to model the soft excess and its variability. For this purpose we require a single model which gives a good fit to each spectra obtained on July 6, 9, and 10. In order to explain the soft excess, the warm edge and reflection models are modified in that the uniform absorbing screen is replaced by a factor representing absorption through a spatially nonuniform region: the so-called partial covering model. When fitting both of these models, the iron line energy was fixed at 6.33 keV and the width was fixed at 0.1 keV. In the following discussions, all quoted χ^2 values correspond to spectra of July 6, 9, and 10, respectively.

First, the warm edge model with the partial absorber was tried with the edge energy fixed at the value of 8.0 keV determined in the previous section. Reduced χ^2 values of 1.2, 1.1, and 1.4 for 16 d.o.f. were obtained which are all marginally acceptable. However, for the spectrum of July 9, the iron overabundance factor is forced to a value below 10^{-2}. This essentially means that the K-edge feature is not found in this spectrum.

The reflection model with the partial absorber was then tried. We obtain excellent fits for all three spectra with reduced χ^2 values of 0.9, 0.7, and 0.8 for 16 d.o.f. The final model is described by

$$F = CE^{-\Gamma}(1 - f_c + f_c e^{-\sigma N_H})[1 + rA(E, \Gamma)] + I_{Fe}$$

where C is the power-law normalization, Γ is the photon index, and I_{Fe} is the line intensity. The first factor modifying the power law represents the partial covering model where some fraction f_c of the power-law source is obscured by a hydrogen column N_H with cross section σ. The derived parameters are listed in Table 2. The values for the reflection normalization are all consistent with the value obtained in the fitting in the 3–28 keV range, although the formal errors here are larger due to the poorer statistics. Within error, the power-law index appears to remain at a constant value of around 2.1 throughout the observation period and is in agreement with that obtained by fitting the model in the 3–28 keV. The steep power law, characteristic of the reflection model, is thus retained when this model is extended to include the softer energy channels.

The partial covering fraction on July 6 and 10 was $\sim$90%. On July 9, where the spectrum was at its softest, the covering fraction fell to an average value of 73%. To further investigate this, we fitted the partial covering model to the spectra obtained on each of the six satellite orbits on July 9. Given the poor statistics in these cases, a reflection component was not included in the model. The free parameters were the power-law normalization, the spectral index, the covering fraction, the hydrogen column density, and the iron line intensity. The variation of f_c on July 9 is shown in Figure 8. The covering fraction is seen to decline from a value of $\sim$80% to a minimum value of $\sim 58^{+7}_{-9}$% and then rise again.

4.3. *Other Possible Origins of Soft Excess*

The partial covering model is very flexible and in many cases can be expected to give a good fit to an observed spectrum where a soft excess is present in the first few low-energy channels. Given that this model fits a spectrum well would not necessarily imply that the soft excess emission does arise through leakage of the power-law emission through a patchy absorbing screen. Unfortunately, *Ginga* is not suited to a detailed investigation of the nature of the soft excess emission. Nevertheless, we consider here other possible origins of the soft excess emission observed in NGC 5506.

In the analysis of the previous *Ginga* observations of NGC 5506, Pounds et al. (1989) fitted a warm 8.3 keV K-edge to the spectrum and suggested that the very small soft excess seen in those observations may be due to absorption through an ionized medium where the opacity below 3 keV is considerably reduced from that of a cold gas. If this warm absorber is produced by irradiation by the central X-ray source, it is natural to expect any variations in the associated soft excess emission to follow variations in the continuum flux. This is not seen in these observations of NGC 5506 where the softness ratio was seen to vary independently of the continuum flux. While we do not rule out the presence of ionized matter in NGC 5506 and

TABLE 2

BEST-FITTING PARAMETERS OF THE COMPOSITE PARTIAL COVERING AND REFLECTION MODEL

Date	C[a]	Γ	N_H[b]	f_c(%)	r	I_{Fe}[c]	χ^2[d]
Jul 6	133^{+52}_{-50}	$2.02^{+0.17}_{-0.12}$	$4.30^{+0.65}_{-0.59}$	$88.4^{+4.0}_{-3.5}$	$1.2^{+1.4}_{-0.8}$	$0.69^{+0.15}_{-0.16}$	0.97
Jul 9	176^{+20}_{-18}	$2.10^{+0.15}_{-0.12}$	$7.82^{+0.83}_{-0.85}$	$72.9^{+3.4}_{-3.6}$	$0.9^{+1.1}_{-0.7}$	$0.52^{+0.15}_{-0.16}$	0.72
Jul 10	267^{+61}_{-64}	$2.14^{+0.11}_{-0.09}$	$4.66^{+0.49}_{-0.44}$	$90.0^{+1.9}_{-1.8}$	$1.2^{+0.8}_{-0.6}$	$0.65^{+0.17}_{-0.18}$	0.86

[a] In counts s^{-1} keV^{-1}.
[b] In 10^{22} H cm^{-2}.
[c] In counts s^{-1}.
[d] Reduced χ^2 for 16 d.o.f.

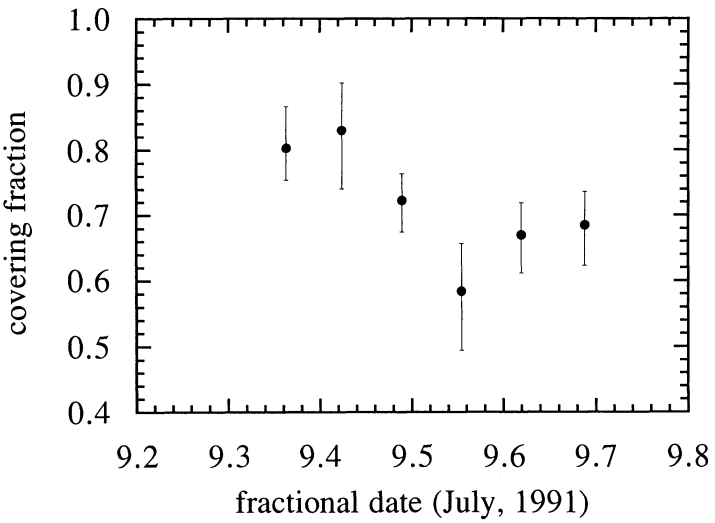

FIG. 8.—Variation of covering fraction obtained from fitting the partial covering model to the spectra of NGC 5506 obtained from each orbit.

that it may contribute to the soft excess, at least in part, we regard it unlikely that the softness variability seen in these observations is due to mechanisms based on photoionization.

The soft excess may be part of the upper tail of a blackbody spectrum. Such a spectrum may be linked with the blackbody spectrum responsible for the so-called UV bump seen in many AGNs or it may represent a second component. In both cases the emission is thought to originate from the inner regions of the accretion disk. We tested a model comprising a power law and a blackbody spectrum, both of which are absorbed by a uniform screen, plus an emission line. We also tested a model comprising an unabsorbed power law and a direct blackbody component and emission line. Both models gave acceptable fits to the spectra of July 6 and 10. However, they both failed to describe the larger soft excess seen in the July 9 spectra. In both models, the reduced χ^2 values were around 3 for 16 d.o.f. Thus we were not able to account for the spectral variability using blackbody models.

We then examined the possibility that the soft excess may arise from a hot plasma in the form of thermal bremsstrahlung. We first tried a model where both the power law and bremsstrahlung components are absorbed and including an additional emission line. This failed to describe the soft excess on all three spectra. The reduced χ^2 values 1.7, 8.1, and 2.8 for 14 d.o.f. for the spectra of July 6, 9, and 10 respectively. We then tried a model comprising an absorbed power law plus a direct thermal bremsstrahlung component and an emission line. We obtained excellent fits for all three spectra if a reflection component is also included and the steep spectrum obtained when fitting the reflection model above 3 keV is retained. The reduced χ^2 values were 1.0, 0.7, and 0.7 for 16 d.o.f. As was the case when fitting the partial covering model, an iron K-edge feature could not be found. Since the fit is only made to the high-energy tail of the thermal bremsstrahlung spectrum, it was not possible to constrain the temperature. In fact, any temperature less than 50 keV gave acceptable fits to each of the three spectra.

The fact that a direct component is required in these models suggests that the bremsstrahlung emission is observed directly from an extended region such as an accretion disk corona. The lack of correlation between spectral softness and the continuum flux seen in these observations would rule out a Compton-heated corona formed by irradiation of the accretion disk by the central X-ray source (e.g., White & Holt 1982). A hot corona may also form through convective turbulence and differential rotation in the accretion disk (e.g. Galeev, Rosner, & Vaiana 1979). It is reasonable to expect any associated variability mechanisms to lie in the accretion disk and to be independent of the central X-ray source. Such a model may be applicable to these observations of NGC 5506.

5. DISCUSSION

From fitting the reflection model in both the 3–28 keV and 1.2–28 keV bands, a steep power-law index of 2.0–2.1 is implied. This is a little larger than the canonical value of 1.9 (Zdziarski et al. 1990). The iron line energy of 6.4 keV and the presence of the reflection feature both indicate cold gas in the system. Given the small absorption column density and the large equivalent width of the iron line, the line is probably produced by fluorescence within the cold, dense gas producing the reflection feature. The observed equivalent width of the iron line of around 200 eV imply large incidence angles of around 80° (Inoue 1989; George & Fabian 1991, Matt, Perola, & Piro 1991). This would tend to favor a clumplike geometry for the cold matter (i.e., blobs or filaments) rather than a disklike geometry.

Considering the results of the partial covering model applied to these observations and the fact that previous observations have shown little or no signs of soft excess emission; it would appear that the covering fraction normally has a value of around 90% or more but declined to ~60% on one episode on 1991 July 9 after which it returned to its normal value. A similar result has also been obtained from an analysis of the spectra of NGC 4151 obtained by *Ginga*, although in this case the dip occurred over a 2 yr time scale (Yaqoob et al. 1993). Also, as pointed out by Yaqoob et al. the existence of a "canonical" value of the covering fraction would rule out the cloud interpretation of the partial covering model since it is hard to realize a situation where a cloud cover can reconfigure itself to a normal state after some disruption such as a temporary break in the clouds. In the case of NGC 4151, a disk interpretation was preferred where the decrease in the apparent covering fraction is the result of an instability in a normally stationary bulk structure.

A similar situaion may be applicable to the variability in the softness of the spectrum of NGC 5506 seen on 1991 July 9. We suggest that the soft excess variability mechanism resides in the inner accretion disk. The flare in the soft excess may arise through instabilities in the inner disk leading to a temporary decrease in the apparent partial covering fraction. Such instabilities may be associated with the process through which dense gas is deposited into the central X-ray emitting region (see Celotti, Fabian, & Rees 1992, for a discussion on the formation of dense gas in AGNs). This variability mechanism would be independent of the central X-ray source and would thus be consistent with the lack of correlation between the softness ratio and the continuum flux. A disk origin of the softness variability is also consistent with the results of fitting the thermal bremsstrahlung model which had suggested the presence of a hot corona formed by instabilities in the accretion flow.

We had argued that observed softness variability is unlikely to arise from mechanisms associated with photoionization such as a absorption through a warm screen. However, since

we do find a warm iron K-edge in the spectral fitting above 3 keV, we do not rule out that the presence of ionized matter in NGC 5506 and its possible importance with regards to soft excess emission. It has been suggested that among Seyfert galaxies in general, the contributions from several sources make up the observed soft excesses (Turner et al. 1991). A realistic situation in NGC 5506 would probably be that the soft excess emission is complex in form and is comprised of at least two components. One component would be associated with the inner accretion disk regions and its variability mechanism located in the same region. Such a mechanism would be responsible for the observations of NGC 5506 reported here. Another component may be associated with photoionization mechanisms and its variability would be coupled to variations in the flux of the central source. Throughout the observations reported here, NGC 5506 remained at a fairly constant intensity with only a slight increase toward the end. Thus it was not possible to check for this type of variability in the present data.

A more detailed look at possible complex features of the soft excess awaits the launch of the next generation of X-ray satellites (*ASTRO-D*, *Spectrum-X*, *AXAF*) which will provide high-energy resolution capability over an extended energy range below 1 keV.

We thank all members of the *Ginga* team for their dedication and support in the observations and data handling.

REFERENCES

Celotti, A., Fabian, A. C., & Rees, M. J. 1992, MNRAS, 255, 419
Fabian, A. C., George, I., Miyoshi, S., & Rees, M. J. 1990, MNRAS, 242, 14
Galeev, A. A., Rosner, R., & Vaiana, G. S. 1979, ApJ, 229, 318
George, I. M., & Fabian, A. C., 1991, MNRAS, 249, 352
Guilbert, P. W. & Rees, M. J. 1988, MNRAS, 233, 475
Holt, S. S., Mushotzky, R. F., Becker, R. H., Boldt, E. A., Serlemitsos, P. J., Szymkowiak, A. E., & White, N. E. 1980, ApJ, 241, L13
Inoue, H. 1989, in Proc. 23d ESLAB Symp., ed. J. Hunt & B. Battrick (Bologna: ESA), 783
Lightman, A. P., & White, T. R. 1988, ApJ, 335, 57
Matt, G., Perola, G. C., & Piro, L. 1991, A&A, 247, 34
Matsuoka, M., Piro, L., Yamauchi, M., & Murakami, T. 1990, ApJ, 361, 440
Morisawa, K., Matsuoka, M., Takahara, F., & Piro, L. 1990, A&A, 236, 299
Morrison, R., & McGammon, D. 1983, ApJ, 270, 119
Perola, G. C., et al. 1986, ApJ, 306, 508
Piro, L., Yamauchi, M., & Matsuoka, M. 1990, ApJ, 360, L35
Pounds, K. A., Nandra, K. A., Stewart, G. C., George, I. M., & Fabian, A. C. 1990, Nature, 344, 132
Pounds, K. A., Nandra, K., Stewart, G. C., & Leighly, K. 1989, MNRAS, 240, 769
Terasawa, N. 1991, ApJ, 378, L11
Turner, M. J. L., et al. 1989, PASJ, 41, 345
Turner, T. J., & Pounds, K. A. 1989, MNRAS, 240, 833
Turner, T. J., Weaver, K. A., Mushotzky, R. F., Holt, S. S., & Madejski, G. M. 1991, ApJ, 381, 85
Urry, C. M., Arnaud, K. A., Edelson, R. A., Kruper, J. S., & Mushotzky, R. F. 1989, in Proc. 23d ESLAB Symp., ed. J. Hunt & B. Battrick (Bologna: ESA) 789
White, N. E., & Holt, S. S. 1982, ApJ, 257, 318
Yamauchi, M., Matsuoka, M., Kawai, N., & Yoshida, A. 1992, ApJ, 395, 453
Yaqoob, T., & Warwick, R. S. 1991, MNRAS, 248, 773
Yaqoob, T., Warwick, R. S., Makino, F., Otani, Y., Sokoloski, J., Bond, I., & Yamauchi, M. 1992, MNRAS, submitted
Zdziarski, A. A., Ghisellini, G., George, I. M., Svensson, R., Fabian, A. C., & Done, C. 1990, ApJ, 363, L1